Old Herborn University Seminar Monograph 15:
Probiotics: bacteria and bacterial fragments as immunomodulatory agents.
Editors: Peter J. Heidt, Tore Midtvedt, Volker Rusch, and Dirk van der Waaij.
Herborn Litterae, Herborn-Dill, Germany: 95-120 (2002).

CHARACTERISATION OF NANOSTRUCTURES OF AUTOVACCINES OBTAINED FROM *E. COLI*

C.A. FAUNCE[1], P. QUITSCHAU[2], M. THIES[3], T. SCHEIDT[3], and H.H. PARADIES[1]

[1]The University of Salford, Joule Physics Laboratory, Institute For Materials Science Center, Manchester, United Kingdom; [2]University of Paderborn, Chemistry and Chemical Engineering, Paderborn, Germany; [3]Hochschule Sudwestfalen, University of Applied Sciences, Biotechnology and Physical Chemistry, Iserlohn, Germany

SUMMARY

Dilute aqueous dispersions of autovaccines have been characterised by transmission electron microscopy, scanning electron microscopy, static and dynamic light scattering and conductivity measurements for volume fractions between $1.0 \times 10^{-4} \leq \emptyset \leq 3.5 \times 10^{-4}$. The static structure factor of the autovaccines molecules depends on the number density of the particles, on temperature, salt concentration, and the nature of counterions, e.g. Ca^{2+}, Mg^{2+}, and 50 -100 mM NaCl. We found that the variation of the particle number density of Lipid A significantly influences the height of the first peak of S(Q) revealing, that the experimentally determined structure factor at low particle concentration shows considerably more structure than expected. The magnitude of the structure factor S(Q) depends strongly on Ca^{2+} ions, rather less on Mg^{2+} ions, but also on the order of the addition of the anions to the autovaccine suspension. We observed small changes in the radii of gyration of the autovaccine suspensions in the presence of Ca^{2+} (11.3 nm) or Mg^{2+} (12.6 nm). The experimental structure factors S(Q) for the various particle densities were analysed in terms of an effective particle charge Z^* and a corresponding screening parameter k^* which were obtained from the Poisson-Boltzmann-Cell (PBC) model. The light scattering data are also in accord with a model, that a small fraction of the ionisable surface sites of the autovaccine which contains phosphate groups, are only partly dissociated (~15%) according to titration and conductivity measurements. It can be concluded that the light scattering data are well represented by a PBC-model of ordering of autovaccines at low volume fractions where colloidal crystals are absent. It was discovered that a given amount of Ca^{2+} (1.0 – 5.0 nM) influences the structure much more than does Na^+ at a considerably higher concentration (0.010 M). This behaviour may explain an ion-exchange mechanism that takes place with Ca^{2+} but at a much lower concentration than for Na^+. Furthermore, the addition of Ca^{2+} at 1.0 – 5.0 nM in the presence of 0.01 M NaCl to the colloidal autovaccine assembly resulted in only small exchange of Na^+ from the sites previously occupied by Ca^{2+}. Comparing the different structure factors S(Q) for Autovaccine-Na^+ and -Ca^{2+}, it

can be concluded that the structure factor does not depend simply on the ionic strength of the solution. The liquid-like interactions at moderate ionic strength, in the presence of Na^+ or Ca^{2+} can be treated as a fluid or polymer electrolyte with a certain degree of ordering in solution, which accounts for S(Q) and the secondary minimum at sufficiently large separation.

Dilute aqueous solutions of autovaccines ($3.5 \times 10^{-3} < Ø < 1.2 \times 10^{-2}$) form stable and regular shaped, colloidal crystals of sizes between 1 to 2 μm. The morphological shapes of the obtained crystals are cubic or rectangular, and by increasing the particle number density of Lipid A above 1.5×10^{-2} they cluster into ordered, long ropes of diameter of 2.8 nm separated by a rope of 4.6 nm having only short range order. The individual cubic crystals are very thin of about 30 nm, and fragile to exposure to the electron beam because of melting. From electron diffraction measurements, various diffraction pattern were obtained, which could be referred to a cubic lattice with a lattice constant of a = 36.14 ± 0.2 nm. In the diffraction patterns obtained from the crystalline specimens of the autovaccines the {110} (d_{110} = 25.50 ± 0.5 nm) reflection is visible and strong, and the diffraction pattern can successfully indexed in a body centred cubic lattice (bcc), with the most likely space group $I\,m\bar{3}m$. In addition, a face centred cubic lattice (fcc) was also found with a = 57.21 ± 0.5 nm occurring at high volume fractions of autovaccines ($0.75 \times 10^{-2} < Ø < 1.2 \times 10^{-2}$) having the possible space group $F\,d\,\bar{3}\,m$ (Q^{227}).

INTRODUCTION

Recently it has been demonstrated that enteric bacteria, e.g. commensurable forms of *E. coli*, are affected through acute or chronic diseases, i.e. bacterial infections in response to foreign and resistant invaders, viral infections and environmental conditions, rheumatism and allergic reactions against mite, different pollens, hair from animals as well as food. Allergic reactions, e.g. dust mite house allergens, storage mites (*lepidoglyphus destructor*) also play significant roles on the formation of distinct pattern of lipopolysaccharides (LPS) of Gram-negative bacteria. The transformation of LPS or Lipid A from commensurable *Enterobacteriaceae* to modified Lipid A molecules includes i.e. magnesium-limited growth and conditions encountered during mammalian infection as reported recently for cystic fibrosis patients after infection with the opportunistic Gram-negative bacteria *Pseudomonas aeruginosa* (*Ernst* et al., 1999).

LPS or Gram-negative endotoxins form the surface of Gram-negative bacteria the major component of the outer leaflet of the outer membrane (*Raetz*, 1990). The major component of LPS is *lipid*, where Lipid A is linked to a core of oligopolysaccharides. Lipid A consists of a β-1,6-linked D-glucosamine (2-amino-2-deoxy-D-glucose) disaccharide carrying six saturated fatty acid residues and one or two negatively charged phosphates at the reducing and non-reducing end of the glucosamine (Figure 1). The basic structure is a β-1' linked D-glucosamine disaccharide which is phosphorylated in position *1* and *4*. Four molecules of R-(-)-3-hy-

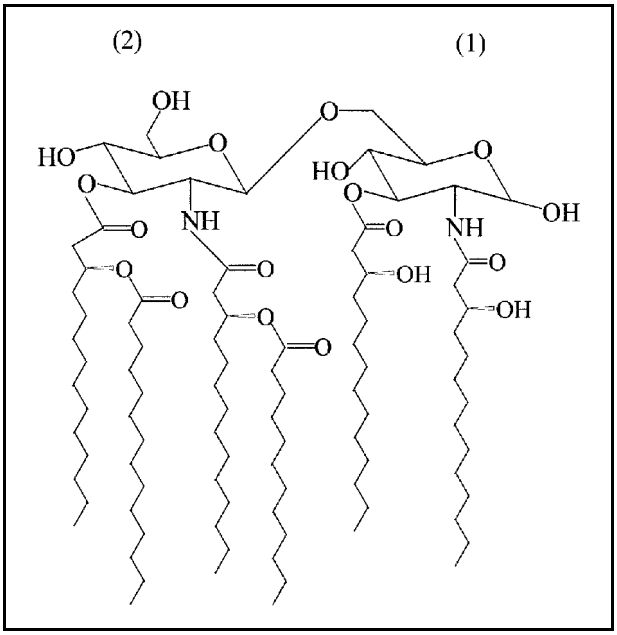

Figure 1: Chemical structure of autovaccines. Chemically, autovaccines consists of a 1,4-di-phosphorylated ß-1,6-linked D-glucosamine disaccharide with four residues of amide and esterified (R)-3-hydroxy fatty acids and carrying two hydroxylated acyl groups. The de-phosphorylated Lipid A is devoid of the inorganic phosphate groups at the reducing and non-reducing end of the disaccharide (see text).

droxytetradecnoic acid are linked to the two glucosamine residues as a backbone. Moreover, each glucosamine (glucosamine *1* & *2*) is substituted by one ester and one amine linked to hydroxy fatty acids. The 3-hydroxy group of the ester linked 3-hydroxytetradecanoic acid of glucosamine *2* is always esterified by tetradecanoic acid, whereas that of glucosamine-N-*1* is not. The amide-bonded 3-hydroxytetradecanoic acid at glucosamine is only substituted with 3-O-aclyted by decanoic acid or tetradecanoic acid while that of glucosamine-N-*1* is only substituted in some cases, mostly by hexanoic acid. The autovaccines so far studied have almost the same chemical pattern, however, some of them do not carry the phosphates, or only one phosphate, and have also been isolated as a mixture of 80% (w/w) of unphosphorylated and 20% (w/w) diphosphorylated Lipid A depending on the history of the disease of the patients (*Paradies* et al., 2000, *Thies* et al., 2001).

The outer membrane is absent in Gram-positive bacteria, hence the structure if the outer leaflet is unique for Gram-negative bacteria. Roughly 3.5 million LPS molecules cover the surface of Gram-negative bacteria, however, the nature of the molecular assembly of LPS in bacteria is of considerable interest in understanding the physical and biological properties of LPS, hence also of Lipid A, because its release in the course of severe infection is the cause of septic shock in patients with endotoxaemia. According to a survey of the Center of Disease Control (Morbidity and Mortality Weekly Report, 1997), this problem caused more than 21,000 mortalities in 1996 in the USA alone.

Moreover, there is considerable interest in understanding of the chemical, biochemical and physical properties of LPS, pyrophosphorylated Lipid A and the phosphorylated forms of free Lipid A, because its release e.g. of free pyrophosphorylated Lipid A in the course of bacterial infections is the cause of septic shock in humans (*Glauser* et al., 1991). Recently a molecular simulation study of LPS has been reported (*Kotra* et al., 1999) visualising the LPS molecule by means of atomic force microscopy (AFM) and molecular simulation, revealing the highest resolution images of any bacterium to date of 50-Å lateral and 5-Å vertical resolution. However, the physical structure of Lipid A (monophosphate & diphosphate) is also of considerable interest, i.e. with potential application in vaccine therapy, compounds known to bind to LPS, which covers the surface of Gram-negative bacteria, chain length dependent agglutination of oligosaccharide clustering by multivalent anion binding, or to find endotoxin inhibitors, which requires the generation of compounds that will prevent cells from overreacting in response to foreign bacterial LPS (*Raetz*, 1996). A complete different application and role in nature is its use as templates for the production of nano-sized materials (*Hinze* et al., 2000; *Clancy* and *Paradies*, 1998), in biomineralisation (*Archibald* and *Mann*, 1993), and drug delivery systems in the presence of double chained cationic surfactants (*Clancy* et al., 1994; *Thies* et al., 1997). In addition, it is contributing to our knowledge of lipid polymorphism (*Mariani* et al., 1988), and the various cubic phases of Lipid A containing systems (*Luzzati* et al., 1992). Therefore, the physical-chemical solution behaviour and its structure in solution of free Lipid A (monophosphate and diphosphate) is of considerable interest in many aspects, particularly prone to their specific transformation in the course of bacterial and viral infections as well as their defence against foreign invaders.

FORMATION OF NANOSTRUCTURES OF AUTOVACCINES IN AQUEOUS SOLUTIONS

The supermolecular structures of LPS have been studied by neutron scattering, small-angle X-ray scattering and electronmicroscopy (*Hayter* et al., 1987; *Seydel* et al., 1987, *Din* et al., 1993, *Brandenburg* et al., 1996; *Seydel* et al., 1993), free Lipid A has been investigated by *Seydel* et al. (1989). None of these studies observed or attributed their experimental findings with the formation of discrete structures in solution, e.g. colloidal crystallisation nor considered to apply many-body effects in solution of Lipid A in terms of colloidal crystals or liquid-like ordering, respectively, although the high potential of these materials to aggregate and the iridescence of these dispersions have been known for a long time. Scattering & diffraction methods (light), e.g. light scattering and small-angle neutron scattering (SANS) are particularly suitable for determinations of sizes, forms and interactions of particles such as the autovaccines in aqueous solutions at different ionic strengths, temperature or in the presence of specific cations e.g. Ca^{2+}, Mg^{2+}, K^{+} and Na^{+}. Autovaccines due to their preparation are colloidal suspensions of dispersed free Lipid A analogue (*Paradies* et al., 2001a) showing highly ordered structures of sizes of ~650 μm in aqueous solutions containing 0.154 M NaCl. This colloidal system exists in a non-equilibrium state, but can be driven into such a state

by application of extremely week forces, by low shear or at very low ionic strength applying tangential ultrafiltration (*Faunce* et al., 2001). Treating the autovaccines as colloidal equilibrium structures and assuming to a first approximation an isotropic distribution of spherical particles, short-range order in this particle distribution can be described by the pair distribution function, g(r), which is proportional to the probability density of finding a pair of particles separated by a distance r. This quantity can also be expressed as an autocorrelation function of the number density fluctuation normalised by the square of the average number density, n, so that g(r) reaches unity at large separations for independent particles. The pair correlation functions are accessible through scattering experiments where the structure factor, S(Q), is measured:

$$S(Q) = 1 + n\int[g(r) - \mathbf{1}]e^{-i\boldsymbol{Q}.\mathbf{r}}\, d^3r \qquad (1)$$

From the normalised measured scattering intensity $I_p(Q) = K\phi a^6 P(Q)$. S(Q), the structure factor, S(Q), can be evaluated as a function of Ø, where Ø is the particle volume fraction and *a* is the radius of this particle. Here, K is a constant depending on the optical properties of the particle and of the solvent. The quantity $Q = |\mathbf{Q}|$ is related to the scattering angle θ by $Q = (4\pi/\lambda) \sin(\theta/2)$, where λ is the wavelength in the suspension. The form factor P(Q), which contains information on the hydrodynamic shape and internal structure of the particle, is the square of the normalised scattering amplitude, B(Q). S(Q), thus contains information about the correlation between particles j and k centred at R_j and R_k, respectively. Equation (1) can be rewritten as:

$$S(Q) = 1 + \frac{1}{N}\sum_{j\neq k}^{N}\sum_{j\neq k}^{N}\left\langle e^{i\mathbf{Q}\cdot(\mathbf{R}_j - \mathbf{R}_k)}\right\rangle \qquad (2)$$

where ⟨ ⟩ denotes the ensemble average and *N* is the total number of particles. For a system of monodisperse particles which interact through strongly repulsive forces, S(Q) reveals a characteristic shape, e.g. at low Q the structure factor is small due to the low value of the osmotic compressibility Υ_T because $S(0) = (1/\beta)\,\Upsilon_T$. For $Q \sim 2\pi\, N^{1/3}$ a characteristic first peak appears, the position of which corresponds to the mean interparticle separation, where g(r) shows a maximum. Moreover, at higher Q, there are less pronounced higher order maxima in S(Q), which decay progressively to unity.

The structure factor, S(Q) was analysed in terms of available liquid state theories (*Hansen* and *McDonald*, 1988; *Oosawa*, 1971; *Roij*, 2000), and an effective pair potential of mean force has to be chosen (*Verwey* and *Overbeck*, 1948; *Hayter* and *Penfold*, 1987), as briefly outlined in this section. For a colloidal system, the potential

$$U(r) = \pi\varepsilon_0\varepsilon_r(2a)^2\psi_0^2\exp[-k(r-2a)]/r, \quad r>2a \qquad (3)$$

is widely used, where r is the center-to-center distance between two particles, ψ_0 is the surface potential, ε_r the dielectric constant of the solvent medium, ε_0 the permittivity of free space, 2*a* the diameter of the particles and *k* is the Debye-Hückel screening parameter. U(r) holds only for low ionic strength

conditions and low particle surface charge density or low surface potential ψ_0. In the dilute colloidal regime of interest here, the interparticle distances are sufficiently large for the interparticle interactions to be given by Equation (3) with an effective or rescaled particle charge Z^* and a rescaled Debye screening parameter k^*. Within this limit, the effective surface potential ψ^*, is related to the effective charge Z* by

$$\psi^* = Z^* /[\pi\varepsilon_0\varepsilon_r(2a)(2 + k^*(2a)] \qquad (4)$$

Since we are interested in the structure of the macro-ion only, an effective one-component description without the degrees of freedom of the small ions is more appropriate. *Medina-Noyola* and *McQuarrie* (1980) showed that within the limit of vanishing macro-ion concentration and for electrolyte ions of vanishing size the mean spherical approximation, yields a screened Coulomb or Yukawa potential of the form:

$$U(r) = \frac{Z^2 e_0^2}{4\pi\varepsilon_0\varepsilon_r}\left(\frac{e^{ka}}{1+ka}\right)^2 \frac{e^{-kr}}{r} \qquad (5)$$

where a is the radius of the particle, e_0 is the charge of the electron and k is the reciprocal Debye screening length, where $k = (\beta e_0^2 \sum_i \rho_i / \varepsilon_0\varepsilon_r)^{1/2}$ and $\beta = 1/k_BT$ is the reciprocal of the thermal energy; the sum here is taken over the univalent counterions and an electrolyte with the bulk number density ρ_i. The solvent enters the interaction potential through its dielectric constant ε_r, only, whereas the macro-ions have an effective charge of Ze_0. For low salt concentrations and higher volume fraction ($0.002 < Ø < 0.02$), Belloni (1993) modified Equation (5), which actually is equivalent to the far-field limit ($r \to \infty$) of the Derjaguin-Landau-Verwey-Overbeck (DLVO) potential (*Verwey* and *Overbeck*, 1948; *Hayter* and *Penfold*, 1987), by applying the mean spherical approximation. The factor $\left(\frac{e^{ka}}{1+ka}\right)^2$ is replaced by a function which depends on ka, Z, and N. Note: In de-ionised suspensions of particles, the radii of which are large compared to the Bjerrum length $l_B = \beta^2 e_0^2 /(\varepsilon_0\varepsilon_r)$, the relative deviation of the above-mentioned factor is not greater than 0.001. For moderate polydisperse systems, the interaction potential between particles having radii of a_μ and a_ν and effective charges Z_μ and Z_ν, Equation (5) can be written as:

$$U_{\mu\nu}(r) = \frac{Z_\mu Z_\nu e_0^2}{4\pi\varepsilon_r\varepsilon_0}\frac{e^{ka_\mu}}{1+ka_\mu}\frac{e^{ka_\nu}}{1+ka_\nu}\frac{e^{-kr}}{r} \qquad (6)$$

For the calculation of the effective charge Z*, or the effective surface potential ψ^* we used the Poisson-Boltzmann Cell model according to *Alexander* et al. (1984) applying a charge renormalisation (*Thies* et al., 2001).

PARTICLE CHARACTERISATION AND POLYDISPERSITY

From the transmission electron micrographs (TEM) the quantities measured in light scattering, e.g. $\overline{R_h}$ and $\overline{R_G}$ are calculated from the moments of the size distribution. For the radius of gyration, the expression $\overline{R_G} = [3\,\overline{R^8} / (5\overline{R^6})]^{1/2}$ was used and for the hydrodynamic radius $\overline{R_h} = \overline{R^6} / \overline{R^5}$ was employed. Assuming that particle interactions can be treated according to Equations (2-6) for volume fractions $1.0 \times 10^{-4} \leq \Phi \leq 3.5 \times 10^{-4}$ and salinities of 10 mM and 100 mM NaCl, $I_p(Q)$ was calculated and its Gaussian distribution, $\rho(x)$, was determined, and the results compared to the experimental values obtained from static light scattering and TEM. The best fit was for an average radius of gyration of $\overline{R_G} = 9.85 \pm 0.50$ nm from the light scattering measurements. The values of $\overline{R_h}$ from TEM were consistently lower by 8.0-9.5%, and 10.0-11.5% lower than the values determined by quasi-elastic light scattering (Table 1, $\overline{R_h} = 13.3 \pm 0.50$ nm). It is not unusual for particle sizes determined from TEM to be smaller than the ones obtained by light scattering, small-angle X-ray scattering or neutron scattering methods because the shrinkage of the hydrated particles caused by the exposure to the electron beam as well as errors in the calibration of the electron micrographs. However, we can not exclude the pos-

Table 1: Summary of the characterisation of the autovaccine particles for volume fractions $1.0 \times 10^{-4} \leq \Phi \leq 3.50 \times 10^{-4}$ at 25°C. The first column lists the number average particle radius $\bar{R}$, the polydispersity ρ_{TEM}, ρ_{LS} and ρ_{QELS}, the radius of gyration $\overline{R_G}$, and the hydrodynamic radius $\overline{R_H}$. The results obtained for 5.0 nM Ca^{2+}, 5.0 μM Mg^{2+} and 50 mM Na^{+} are included. The second column summarises the quantities calculated from the size distribution corrected for polydispersity with respect to the independently measured quantities, and the average weight molecular weight, $\overline{M_w}$, the ratio of weighted average molecular weight to number averaged molecular weight $\overline{M_n}$, $\overline{M_w} / \overline{M_n}$*.

	Quantity (uncorrected)	Size distribution independently (corrected) determined	Size distribution measured
R/ nm	11.5 ± 0.30	12.64 ± 0.30	……
ρ_{TEM}/ %	8.0 ± 0.60	8.70 ± 0.60	……
R_H/nm (QELS)	13.3 ± 0.70	12.95 ± 0.50	13.40 ± 0.55
R_H/nm, (QELS), Ca^{2+}	14.5 ± 0.50	14.48 ± 0.50	14.50 ± 0.50
R_H/nm, (QELS), Mg^{2+}	15.5 ± 0.80	15.40 ± 0.60	15.65 ± 0.55
R_H/nm, (QELS), Na^{+}	14.2 ± 0.30	14.30 ± 0.50	14.35 ± 0.40
R_G/nm (LS)	10.5 ± 0.30	9.80 ± 0.30	9.85 ± 0.55
R_G/nm (LS), Ca^{2+}	11.3 ± 0.30	11.00 ± 0.40	11.10 ± 0.50
R_G/nm (LS), Mg^{2+}	12.6 ± 0.45	12.00 ± 0.55	12.00 ± 0.50
R_G/nm (LS), Na^{+}	10.9 ± 0.50	10.50 ± 0.60	10.80 ± 0.63
ρ_{LS}/%	5.0 ± 0.70	5.00 ± 0.70	……
ρ_{QELS}/%	5.7 ± 0.75	5.75 ± 0.75	……
$\overline{M_w} \cdot 10^6$/gmol^{-1}	3.75 ± 0.86	3.69 ± 0.75	3.60 ± 0.40
$\overline{M_w} / \overline{M_n}$	1.032	1.032	1.025

* $\overline{M_n}$ was obtained from osmotic measurements (Knauer Membrane Osmometer, 15,000 MW membrane; *Paradies*, unpublished).

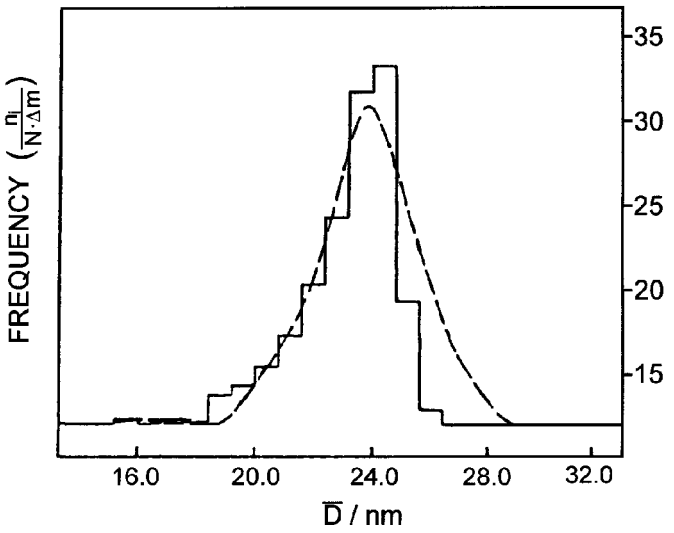

Figure 2: Size distribution of Lipid A aggregates obtained by transmission electron microscopy. Full line histogram, original data: dashed line is the smoothed distribution calculated from the histogram with the average radius of $\bar{R}$ = 12.64 nm and polydispersity ρ = 8.7%.

sibility that the differences between the radii of TEM and static light scattering could be attributed to the polydispersity of the system. Figure 2 shows the size distribution of the autovaccines, whereas Figure 3 illustrates autovaccine particles at a volume fraction Ø = 2.5 x 10^{-4} revealing spherical particles of average diameters of d ~25 nm at low salt (0.005 M). Figure 4 shows SEM electron micrographs of colloidal crystals of autovaccines obtained at volume fractions of Ø = 3.5 x 10^{-4} and 4.0 x 10^{-4}, respectively. Using the radius obtained from the TEM and a size distribution with the normalised variance $\overline{\rho_{TEM}}$ = 7.1 ± 0.8%, an estimate of the hydrodynamic radius was calculated to $\overline{R_h}$ = 12.50 nm from the radius of gyration which shifted the size distribution by 8.5%. Reasonable agreement can be found between $\overline{R_h}$ and $\overline{R_G}$, the values obtained from TEM and the light scattering experiments, respectively. This results in an average of $\overline{R_h}$ = 12.64 ± 0.2.5 nm and a polydispersity of $\overline{\rho_{TEM}}$ = 8.7 ± 0.6%. According to *Pusey* (1980) the particle polydispersity, ρ_P, can be expressed as

$$\rho_P = \sigma / a \qquad (7)$$

and set to ρ_P < 5% as a criterion for a system which can be treated as a one-component system. Applying this criterion for polydispersity, we calculate, for the TEM results, a value of 6.4% for ρ_P, which is consistent with the value found from light scattering measurements of 9.5%. As has been pointed out by *Hayter* and *Penfold* (1991) it appears that a higher degree of polydispersity can in fact be accepted for charged particle systems.

Furthermore, it should be noted that the TEM electron micrographs may give a false impression that a Gaussian distribution is appropriate where in fact the distribution could have been a log normal, where a tail exists extending to smaller particle sizes even though we could not detect any significantly smaller particles. If this were the case, the particle size distribution parameter could still be higher than 8.7 ± 0.6%. Applying a log normal distribution of

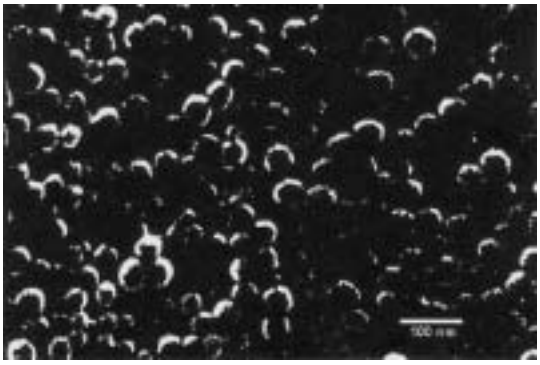

Figure 3: SEM electron micrograph of Lipid A aggregates at a volume fraction of Ø = 2.5×10^{-4}. The size bar is 100 nm.

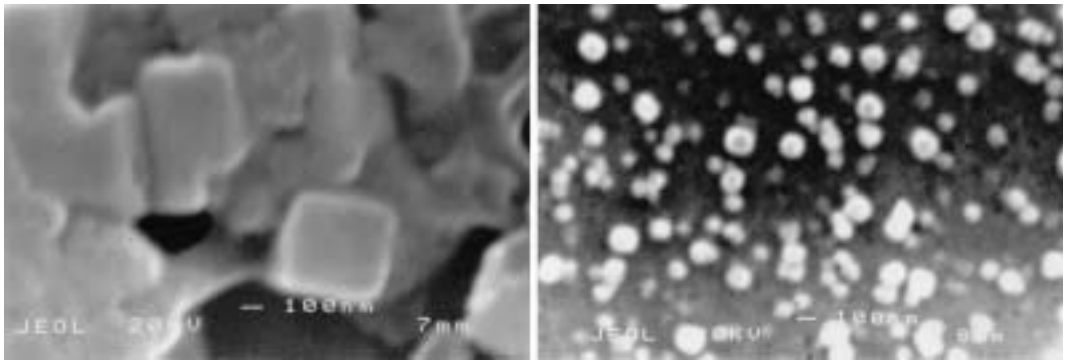

Figure 4: SEM electron micrographs of colloidal crystals of Lipid A obtained at a volume fraction Ø = 4.0×10^{-4} (left), and at a volume fraction Ø = 3.5×10^{-4} (right), showing large colloidal crystals. The size bar is 100 nm.

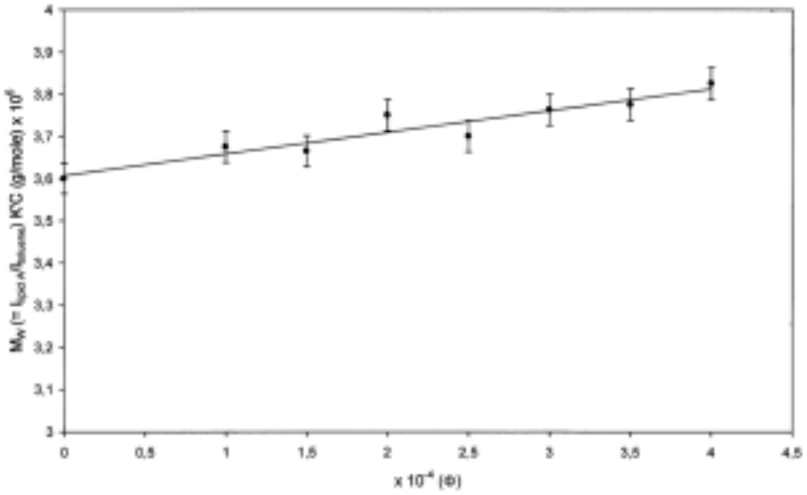

Figure 5: A plot of $I_P / K' c \cdot I_{toluene}$ vs. volume fraction Ø yielding a molecular weight of $M_w = (3.6 \pm 0.4) \times 10^6$ g/mol in the presence of 1 mM NaCl and Q = 2.5×10^{-2} nm^{-1}.

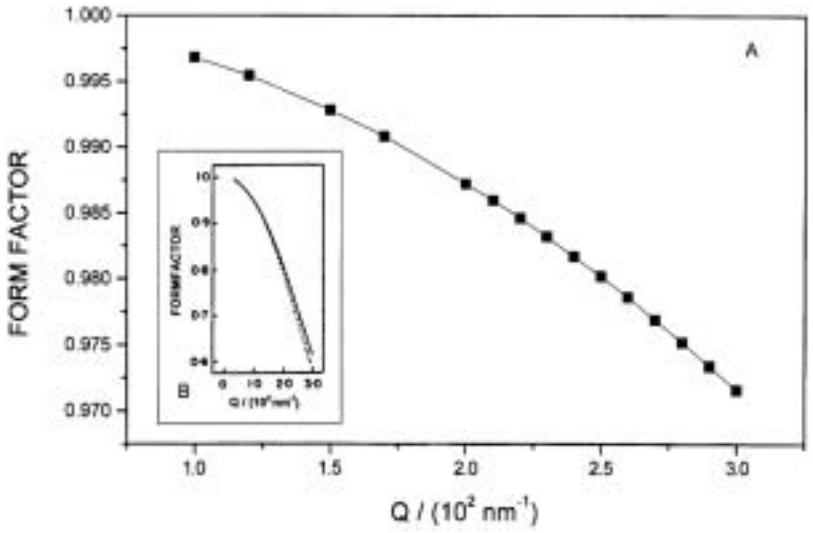

Figure 6: (A) Experimental particle form factor of Lipid A (◆····◆) and best fit calculation applying the Guinier approximation with $\overline{R_G}$ = 10.1 nm.
(B) Guinier approximation for a polydisperse form factor (8.7%) calculated with Mie theory as a homogeneous sphere with complex index of refraction r = 1.532 + i 0.0015. The dotted line is the prediction with ρ = 8.7% and $\overline{R}$ = 12.64 nm.

the particle size polydispersity recalculated from the M_w distribution, we found a value of the order of 8.5±0.7%.

The weighted-average molecular weight, M_w, for the volume fraction in the range $1.0 \times 10^{-4} \leq Ø \leq 3.50 \times 10^{-4}$ was determined in the presence of 1.0–100.0 mM NaCl by plotting $(I_P / K' c \cdot I_{toluene})$ vs. Ø (Figure 5), revealing a slight positive slope indicating a repulsive potential between like-charge species which is almost independent of the range of the volume fraction studied ($1.0 \times 10^{-4} \leq Ø \leq 4.0 \times 10^{-4}$), and yields after extrapolation to Ø = 0, $M_w = (3.60 \pm 0.40) \times 10^6$ g/mol, $N_{agg} = 2.2 \times 10^3$, $K_{as} = 10^{8.5}$ L/mol (Table 1). The positive slope does not preclude the possibility that excluded volume effects are not present, for this would give rise to repulsive interactions for any type of particles whether they are charged or not. However, the repulsive interactions would be less sensitive towards addition of salt.

STRUCTURE FACTORS

The structure factor S(Q) was extracted from the average intensity by normalising I(Q) to the average particle form factor P(Q). One of the main problems of this technique for polydisperse suspension compared to monodisperse ones is an increase in scattered intensity at low Q values which makes precise measurements difficult for dilute suspensions. This, of course, can lead to considerable errors in S(Q). However, as outlined above, by applying the polydispersity criterion of *Pusey* (1980) we can treat this dilute suspension to a one-component system to a first approximation for extraction of the form factor P(Q) from I(Q). Considering that we have strong interactions in the dilute

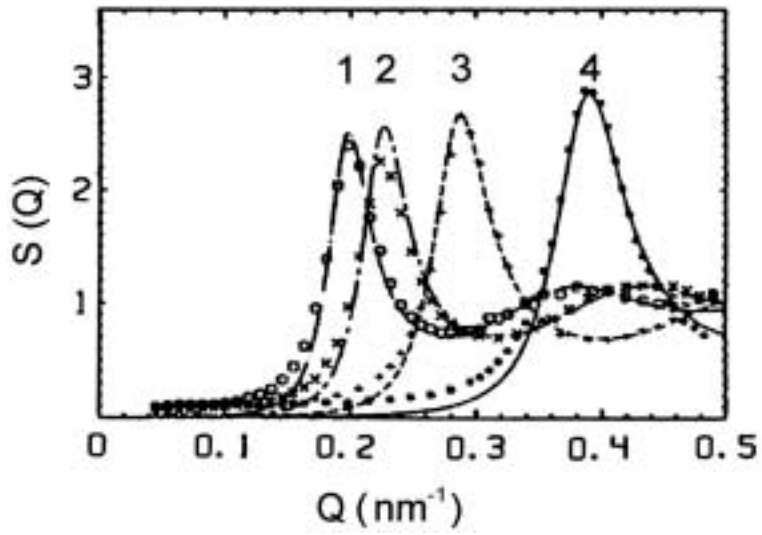

Figure 7: Experimental structure factors S(Q) as obtained from the PBC model and the RSMA for different particle number densities: 2.45 x 10^{15} particles/ml (1); 3.05 x 10^{-4} particles/ml (2); 3.9 x 10^{15} particles/ml (3) and 4. 9 x 10^{15} particles/ml (4).

system in the absence of salt as well as at low salinity e.g. 10 mM NaCl, it is safe to calculate the form factor P(Q) according to Guinier's approximation (*Guinier*, 1955), since the compressibility (χ) for a particle with a = 12.64 nm amounts to 0.0067 for a monodisperse system in the absence of salt, and 0.0063 for a polydisperse system after allowing for the determined polydispersity index. The experimentally obtained radius of gyration was used, $\overline{R_G}$ = 9.80 ± 0.55 nm (Table 1), to normalise the form factor, and then P(Q) vs. Q was calculated according to the Guinier approximation as shown in Figure 6 together with the experimental data and compared with the form factor calculated using the Mie theory assuming a homogeneous sphere having a hydrodynamic radius of $\overline{R_h}$ = 12.64 nm with a complex index of refraction r = 1.532 + i0.0015. Figure 7 shows a series of examples of measured structure factors, S(Q), with different volume fractions for the *Autovacccine* suspensions in water after applying the PBC model and the rescaled mean spherical approximation (RSMA) according to *Hansen* and *Hayter* (1982).

The effective charges and volume fractions were determined by fitting the positions and heights of the peaks in the calculated structure factors S(Q) to the experimental scattering data. The structure factor, S(Q), was calculated using the (RSMA) algorithm as a convenient tool to generate theoretical structure factors for comparison with the experimentally obtained structure factors, S(Q), particularly for these dilute suspensions assuming an average particle radius of $\overline{R_h}$ = 12.64 nm and a polydispersity of ρ_{LS} = 5.0%. In comparison, the volume fractions found ranged from 1.15 x 10^{-4} to 3.75 x 10^{-4}, and were surprisingly close to the ones calculated from dilution experiments. Within this volume fraction range, the effective charges were determined to be of the order of Z^* ~ 373-460 grouping around 400 for a bare particle charge of Z_P = 780 and for $\overline{R_h}$ = 12.64 nm. Table 2 lists the parameters for calculation of the structure factors, S(Q), of this Lipid A dispersion for a particle density of

Table 2: PBC model with effective charge Z^*_p and effective reduced, screening parameter $k^*/(2a)$ for various particle density numbers and for a fixed charge of $Z_P = 800$

Number density (particles/cm^3)	Z^*_p	$k^* \cdot (2a)$
1.5 x 10^{15}	421	0.21
2.0 x 10^{15}	400	0.23
2.5 x 10^{15}	378	0.25
3.0 x 10^{15}	360	0.28
3.2 x 10^{15}	348	0.37
3.5 x 10^{15}	300	0.47

1.25 x 10^{15}/cm^3 and particle diameter of d = 25.28 nm. Note: The effective charges obtained from a mono-disperse fit to the light scattering data after applying the (RSMA) closure for calculating the structure factor, the true effective charges can be underestimated by underestimating the colloidal structure due to polydispersity.

These effective charges and the volume fractions $\kappa a > 0.1$, and the deviation from the pre-factor in the Yukawa potential, were found to be of the order of 10^{-3}. Moreover, Figure 7 shows structure factors, S(Q), for four different particle number densities of Lipid A suspensions which are close to $\Phi \cong 3.0 \times 10^{-4}$, ranging from a particle number densities from 2.45 x 10^{15}/cm^3 to 4.9 x 10^{15}/cm^3 and again the effective charge values Z* cluster around $Z^* \cong 390$ - 410. The appearance of the structure factors, S(Q), for these various number densities and the height of the first peak do not change significantly in the presence of 10 mM to 50 mM NaCl. The height of the first peak in all the S(Q) curves is well above 2.0 as it is also the case for the structure factors, S(Q), for all volume fractions. According to the rule of *Verlet* and *Hansen* (1969), crystallisation occurs as the structure factor of ordinary liquids exceeds a value of 2.85. This effect is seen especially for autovaccine particles having a number particle density of 4.0 x 10^{15} particles/cm^3. Here, an increase in height of S(Q) and a shift towards higher Q-values even occurs at volume fractions as low as $\Phi \cong 1.50 \times 10^{-4}$. The situation does not change significantly upon increasing the ionic strength to 50 mM NaCl, or 100 mM NaCl as long as the number particle density is below ~5.0 x 10^{-4}. However, a significant ordering of the autovaccine particles at this low volume fractions of ~1.50x10^{-4} in the presence of 100 mM NaCl (25°C), or 5.0 nM Ca^{2+} and 50 mM NaCl, respectively, results in a significant increase in height of S(Q) to 3.0. Indeed, this solution does show a strong tendency to crystallise sometimes into colloidal crystals of sizes up to 1.5 – 5.0 μm. After stirring (2-3 hrs) or heating the solution (20-30 s) to 50°C, these colloidal crystals of autovaccines dissolve, which can also be monitored in a UV-VIS spectrophotometer at ~540 nm due to changes in the transmission. Furthermore, in the calculation of S(Q), the charge $Z_\mu$of component μ has been taken into account (Equation 5 and 6), because Z_μ scales with a^2_μ. The values of S(Q) were calculated for $Z_\mu \propto a_\mu$ keeping the average charge constant. No significant polydispersity was found with respect to the width and height of the first peak, once again indicating that the polydispersity does seem to be rather low.

The total anionic charges of 5940 per particle, the experimentally determined exposed surface charges per particle of

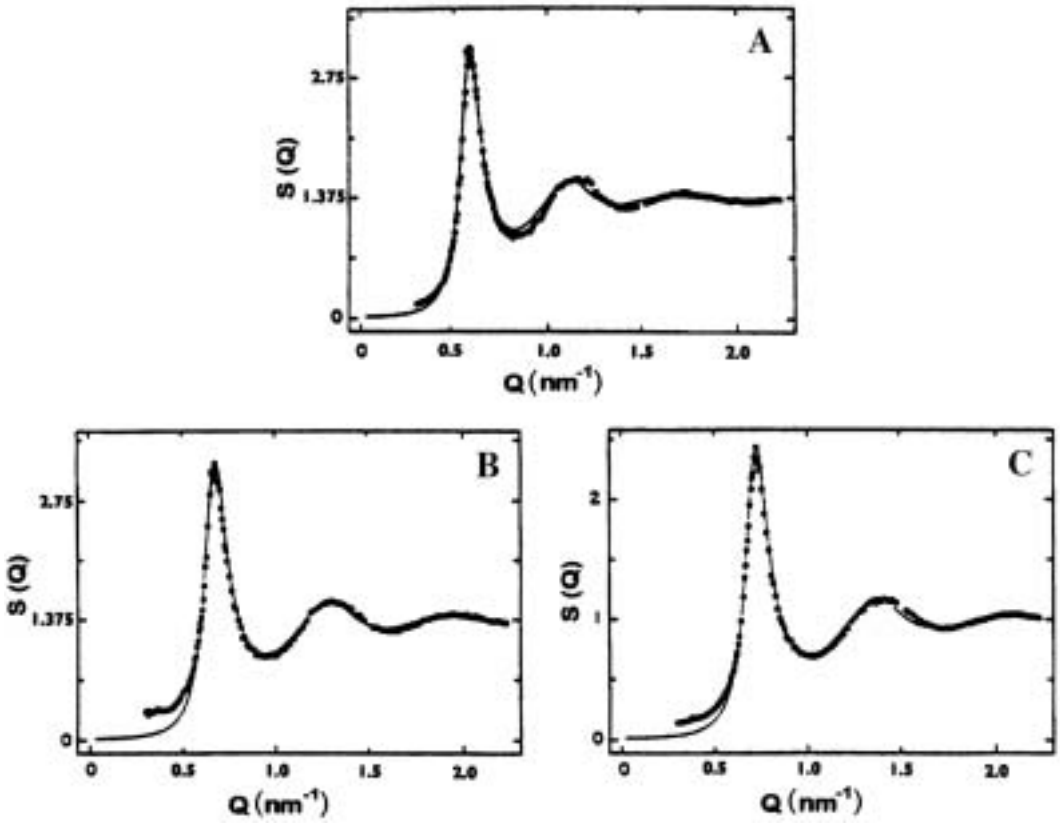

Figure 8: Experimental structure factors S(Q) as obtained from the PBC-model and the RSMSA, for a particle density of 1.60 x 10^{15}/ml in the presence of 5.0 nM Ca^{2+} (A), 3.5 nM Ca^{2+} (B), and 2.5 nM Ca^{2+} (C). Experimental structure factors (• --- •) and calculated ones (full line) according to the PBC model.

~380 including the bound protons (~60), which remain electrostatically bound to the particle, and the determined pK_a value of 7.21 of the autovaccine suspensions enables us to study the interactions of Ca^{2+} and Mg^{2+} with the negatively charged Lipid A and to study their influence on the structure factor S(Q). This interaction is among other biological actions a process of utmost biological significance due to

1) it is the biochemical mechanism by which Lipid A influences plasma levels of various interleukines (*Ernst* et al., 1999);
2) due to the increased stimulation of susceptibility to innate immune killing, and
3) the significant decrease of inflammatory response in the presence of autovaccines or Lipid A derivatives from clinical isolates and laboratory strains grown in low Mg^{2+} medium.

The autovaccine suspensions have been studied in the same volume fraction and number particle density as described before, but in the presence of 1.0 – 5.0 nM Ca^{2+}, 1.0 – 5.0 μM Mg^{2+}, and as a mixture of both at the same molarities (*Paradies* et al., 2001). Figure 8 shows the structure factor, S(Q), for a number particle density of 1.6 x 10^{15}/cm^3 in the presence of 1.0, 2.5, 3.5, and 5.0 nM Ca^{2+}, which were added as $CaCl_2$ to the Lipid A suspension. It is interesting to observe, that here the height of the first

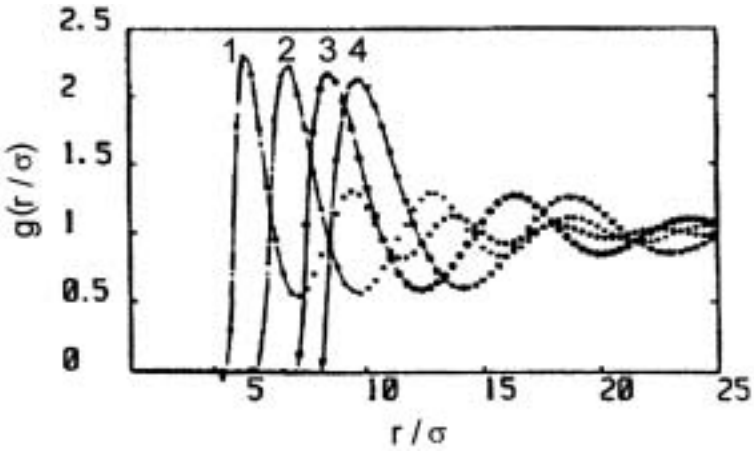

Figure 9: Radial distribution function g(r) for different particle concentrations: 2.5 x 10^{15} particles/ml (1); 3.5 x 10^{15} particles/ml (2); 4.0 x 10^{15} particles/ml (3), and 4.9 x 10^{15} particles/ml (4) obtained by Fourier transformation of the measured S(Q).

peak of S(Q) exceeds the value of 2.85 according to the Hansen-Verlet melting rule by a factor of 1.16. At low Q, the structure factor S(Q) approaches a constant value different from zero, which might be due to polydispersity of the Lipid A suspension in the presence of Ca^{2+}. It can be seen from Figure 8, that increasing the Ca^{2+} concentration above 3.5 nM gives no further increase in height of the first peak. No significant effect on the magnitude of the structure factors, S(Q), can be noted after adding 50 mM or 100 mM NaCl to this sample. However, when the same experiment is conducted in the reverse order, e.g. adding the NaCl solution (50 mM or 100 mM,) prior to the 1.0 nM – 5.0 nM Ca^{2+} solution, a significant decrease in the height of the structure factor S(Q) was observed by a factor of ~1.9. This indicates a loss of structure when compared to the structure factors S(Q) of the autovaccine suspensions in pure water or low NaCl solutions. Addition of concentrations higher than 3.5 nM up to 15.0 nM Ca^{2+} have no detectable effects on the magnitude of the structure factor, S(Q). Furthermore, determinations of the form factor as a function of scattering vector as well as the radius of gyration as determined of these suspensions of autovaccines, did not change in comparison to those determined for the free Lipid A suspensions in the absence of salt (Table 1).

Pursuing the same experiments in the same order as the ones conducted for Ca^{2+} but with Mg^{2+}, using much higher concentrations than for Ca^{2+}, of the order of 1.0 – 5.0 μM, a significant loss of structure was observed, which can be reversed with the addition of 50 mM or 100 mM NaCl, to yield almost the same value of the structure factor S(Q) as before the experiment was started in the presence of 50 mM salt. Alternatively after two hours, the same value for the structure factor S(Q) can be recovered having the same magnitude and appearance as in Figure 9. Moreover, no change was noticed at higher Mg^{2+} concentrations as long as the temperature is kept at 25°C. It would appear, that the addition of Mg^{2+} in the presence of 50 mM or 100 mM NaCl results only in a small decrease of the height of the structure factor S(Q), which does not change with time (24 hrs) at constant temperature. However, the radius of gyration for this system changed to a higher value (12.6 nm) unlike the one

for Ca^{2+} which was 11.3 nm (Table 1). However, we observed that colloidal crystallisation of the autovaccines occurred already at volume fraction of 1.7 x 10^{-4}.

Adding 5.0 nM Ca^{2+} and 5 μM Mg^{2+} to the de-ionised Lipid A suspension with a number particle density of 1.6 x $10^{12}/cm^3$, the same appearance with respect to magnitude of the structure factor S(Q) and position is observed as for Ca^{2+} alone, so what matters is the order of addition, e.g. with Ca^{2+} first then Mg^{2+}, the structure factor S(Q) for Ca^{2+}-autovaccine is unaffected by Mg^{2+} at all. The addition of salt solutions of the order of 50 mM NaCl or 100 mM NaCl to this suspension does not affect the magnitude of the structure factor S(Q) if the temperature is kept at 25°C. No changes in the radius of gyration (R_G = 12.6 nm) or in the polydispersity index were observed in the presence of the 5.0 nM Ca^{2+} and 5 μM Mg^{2+}. The dissociation constant of Ca^{2+} of K_d = 2.4 nM is much lower than for Mg^{2+} K_d = 9.7 μM, indicating that binding of Ca^{2+} is much stronger than the one for Mg^{2+}, which implies preferential binding of Ca^{2+} over Na^+ and Mg^{2+} ions. Removing the Ca^{2+} through the addition of 5 mM EDTA and extensive dialysis in the presence of 10 mM NaCl, the same structure for the autovaccines is seen. It is quite surprising that Ca^{2+} ions at such low concentrations do improve ordering of the Lipid A clusters in solution to such an extent, and that neither Mg^{2+} nor Na^+ ions are able to exchange Ca^{2+} (*Paradies* et al., 2001).

It is apparent that Ca^{2+} sites must select Ca^{2+} in preference to the much more numerous Na^+ ions present in solution, even though the two cations have precisely the same diameter. The Lipid A or the autovaccines obviously bind Ca^{2+} very tightly with K_d = 3.5 nM as opposed Mg^{2+} = 1.5 mM, and upon doing so, blocks Na^+ binding to some extent. This still raises the problem as to how Ca^2 ions pass through the Lipid A or autovaccine aggregate to their binding sites without some change in the shape of the Lipid A or autovaccine molecule. Since the form factor P(Q) and the dependence of P(Q) on Q (R_G = 10.21 ± 0.8 nm, Figure 6), or the size distribution observed by TEM or SEM of the autovaccine aggregate in the presence of 5.0 nM Ca^{2+}, and the weighted average molecular weight ($\overline{M_w}$ x 10^6 = 3.85 ± 0.9) does not change at all as observed here. It may be assumed according to the titration data that the binding sites for Ca^{2+} or Mg^{2+} are not only located on the surfaces of the dispersed Lipid A colloids. Another explanation can be offered analogous to the one for the binding sites of Ca^{2+} or Mg^{2+} like EDTA chelators, considering the favoured pK_a at low pH (5.5 – 6-5) where no phosphate groups are involved. A model can be constructed which permits eight oxygen atoms, each built with charge of –1/2 and Ca^{2+} to float freely in a confined volume with a dielectric coefficient, so that the oxygens then interact with ions that pass in and out of the volume, always acting to maintain electroneutrality within this space. This would explain the retention of the number of surface charges in the presence of the Ca^{2+} as well as the insignificant change on the surface charges of Na^+. Moreover, the almost constant surface charge of 350 ± 70 found for Na^+ in the presence of Ca^{2+}, and the small reduction of surface charge after addition of Na^+ from 350 ± 70 to 200 ± 50 in the presence of Ca^{2+}, may have its origin in the replacement of two Na^+ by one Ca^{2+}, leaving approximately 70 – 80 Ca^{2+} ions located at the surface. Titration of these Ca^{2+} ions by an ion selective electrode as well as by a Ca^{2+} specific indicator yielded values of 76 ± 10 Ca^{2+} ions, the rest of the Ca^{2+} ions are apparently located in the interior of the

Table 3: Variation of the total and of the effective charge of the autovaccines with added NaOH at constant volume fraction Ø = 3.5 x 10^{-4}. The surface parameters at low salt concentrations (5 mM NaOH) are: Total surface charge density ρ_T = - 0.12 C/m^2, effective particle radius α = 12.8 nm, Stern capacitance, C_S = 0.48 F/m^2, pK_a of the phosphate group is 7.20, and α is the degree of dissociation.

[NaOH]/M	pH0	pHd	Z	Z*	Φ0/mV	α
10^{-7}	1.51	5.70	900	170	- 230.4	5.40 x 10^{-4}
10^{-6}	1.66	6.55	950	200	- 250.3	5.10 x 10^{-4}
10^{-5}	3.46	8.51	1010	210	- 263.5	2.78 x 10^{-2}
5.0 x 10^{-5}	4.66	9.31	1200	215	- 290.3	1.50 x 10^{-1}

cluster, and possibly chelated within the region of the chiral (R)-3-hydroxyoctanoic acid residues of the colloidal suspension of Lipid A.

The low affinity of Mg^{2+} compared to Ca^{2+} can be related to the ability of Mg^{2+} to bind water unusually tightly. Also it is noteworthy that the Ca^{2+} associated strongly with this autovaccine can be found analytically in MALDI-TOF-mass-spectroscop, by Ion Spray-mass-spectroscopy, or by combined Capillary electrophoresis and MALDI-TOF in the same total amount after extensive dialysis or electrodialysis against water, and by calculating the difference in the average number of charges of the calcium bound Lipid A (250, 265 for the autovaccines) prior to addition of sodium chloride or vice versa. The strong influence of Ca^{2+} ions on the solution structure, S(Q), may have also reflect the observation, that the autolysis of the autolysine-susceptible cell walls of *Staphylococcus aureus* during growth is dependent on low Ca^{2+} but in the presence of high salt (*Ochiai*, 1999; 2000).

SURFACE CHARGE

Preliminary data on particle surface charges were determined by comparing $S_{eff}(Q)$ obtained from light scattering for diluted systems having volume fractions of 1.5 x 10^{-4} ≤ Ø ≤ 2.0 x 10^{-4}, from values obtained by fitting to the PBC model. The fitting procedure yielded an average surface particle charge of 400 ± 80 in the presence of 50 mM NaCl, close to that deduced from conductivity measurements. No significant differences were noticed between the low salinity (1.0 mM, 410 ± 70) and high salinity (100 mM, 395 ± 70) solutions (*Thies* et al., 2001). From the results obtained when NaOH was added to the autovaccine suspensions during titration and conductivity measurements, and by applying the PBC model, predictions were made of the effective charges at intermediate salt concentrations (Table 3).

Basically, free protons are excluded from the surface of the colloidal Lipid A particle, so when using the Stern model, $[H^+]_0$ has to be replaced by the proton concentration at the outer Helmholtz plane according to the equation:

$$[H^+]_d = [H^+]_b \cdot e^{\Psi} \quad (8)$$

This expression includes the dissociation of the phosphate, where the concentration is given as volume concentration and the subscripts of d, b and s mean the concentration in the diffuse layer, the bulk solution and in the Stern layer, respectively, as defined by Equation (9):

$$K_{R\text{-}O\text{-}P(=O)(OH)_2} \cdot e^{\beta\sigma/C_S} = [R\text{-}O\text{-}P(=O)(OH)O^-] \cdot [H^+]_d / [R\text{-}O\text{-}P(=O)(OH)_2] \quad (9)$$

where σ is the total charge density and C_S the Stern capacitance. Table 3 lists the variation of the effective charges as the suspension of the autovaccines is titrated with NaOH at a constant volume fraction of $\Phi = 2.0 \times 10^{-4}$. The effective charges were obtained from the PBC model. The corresponding effective charge, $Z^* = 215$ at the highest NaOH concentration used (5.0×10^{-5} M) is significantly lower than the saturation value of ~400 predicted by the BPC model. Using the criteria by *Alexander* et al. (1984), it has been found, that if $Z^* = 215$ is taken as the structural particle charge for the linearised Poisson-Boltzmann equation predicts a value of 170 at 50 mM salt, and at 200 for 100 mM salt. This would imply, if all sites were charged, a surface charge of 400 sites/particle for this suspension. However, the bare charges of this suspension increase with NaOH concentration at constant volume fraction primarily due to the resulting increase of the pH. The observed discrepancy between the number of total charges (~400) and the structural colloidal charge of ~170 – 200 detail, one has to increase the volume fractions, use small-angle light scattering techniques, and small-angle X-ray scattering. However, the use of scattering techniques is also limited since the autovaccine particles form colloidal crystals at higher volume fraction.

It is thus clear that indicates that only half the fraction of the available sites is ionised. So, with the inclusion of the charge regulation, the resulting effective charges are always lower than their saturation values in the absence of charge regulation. To investigate the surface charges of this colloidal aggregate in more further detailed study of the dynamics of the ordered structure of Lipid A or the autovaccines in the presence of both Ca^{2+} and Mg^{2+} ions is most desirable, particularly to help us to understand changes in the physical surface charges, their salt-, pH- and temperature dependence, as well as their dependence on higher number densities of solute. Moreover, there is strong evidence that this ordered structure of the autovaccines in aqueous solution is stable over several months when the Lipid A concentration is maintained within the relevant volume fraction range.

Having established the spherical size of the autovaccines with diameters of d = 24.5 nm and the onset of crystallisation at volume fractions of $\Phi = 3.5 \times 10^{-4}$, we should expect close packed arrays of spheres of free Lipid A or autovaccines. These systems, termed colloidal crystals, are composed of either polymer like polystyrene sulphonates, viruses such as *Tipula iridescent virus* (TIV) suspensions (*Klug* et al., 1959) or free Lipid A and autovaccines, which have been shown for the first time under strictly controlled conditions to form these crystalline structures (*Thies* et al., 2001; *Paradies* et al., 2000; *Faunce* and *Paradies*, 2001; *Paradies* et al., 2000, *Faunce* et al., 2001). Like the natural gem stone opal they diffract light as a result of the submicrometer diameters of these colloids (*Hiltner* and *Krieger*, 1969; *Luck* et al., 1963**;** *Hachisu* et al., 1973; *Asher* et al., 1998), where the colloidal crystals of free Lipid A or autovaccines spontaneously form under ambient conditions as reported before.

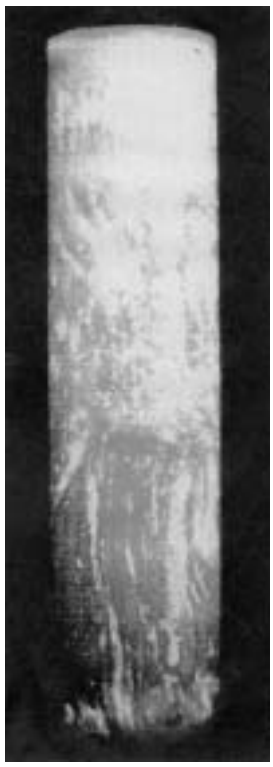

Figure 10: Image plate photograph of colloidal crystals of autovaccines at ionic strength of 0.0005 M (25°C) after coating with C_{16}-fluorescein thiocynate, showing Bragg reflections in dimethylsulphate/water, 70/30 (v/v).

FORMATION OF COLLOIDAL CRYSTALS OF THE AUTOVACCINES

Above a volume fraction of Ø = 3.5 x 10^{-4} at low salt (I=0.0001 M), or in the presence of 0.150 M NaCl, however at Ø =1.5 x 10^{-4}, colloidal crystals of the autovaccines are appearing (Figure 3), whereas Figure 10 shows colloidal crystals of autovaccines, which have been doped with fluorescein thiocyanate (C_{16}) and illuminated with laser light of λ = 621.1 nm, revealing intense Bragg reflections of pseudo-hexagonal closed packed (hcp) colloidal crystals of autovaccines. These colloidal crystals, sometimes of sizes of 2 and 5 μm but rather thin (50 nm in thickness) form only if a narrow size distribution of the particles is preserved. When these colloids settle into surface features, quite a few structures can be generated as it has been observed in TEM and electron diffraction pattern as well as in Atomic Magnetic Force Scanning Electron microscopy (AMF). These 2D patterns can be used to build up 3D colloidal crystals. Other forms or approaches e.g. for Lipid A or the autovaccines exploit the complex phase diagram of colloidal mixtures (*Faunce* et al., 2001). When colloids of different sizes are allowed to crystallise together, they can form a variety of different crystal structures depending on the sphere size and its

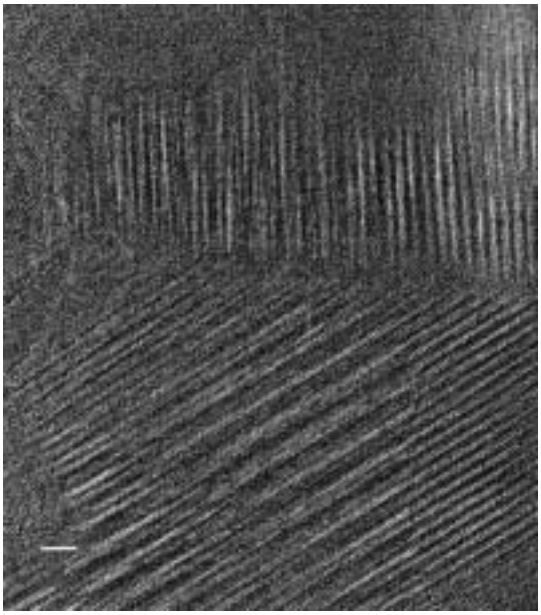

Figure 11: TEM image of unprocessed resolution of autovaccine showing three sets of lattice rows. The image shows also at least two domains of different orientations (likely twinned), and superimposed lattices of two domains. The bar scale is 25 nm (*Faunce* and *Paradies*, unpublished results).

polydispersity index, and particle number density rather than mass. Figures 11 - 14 show molecular resolution images obtained from TEM diameters of 2.75 – 2.80 nm, separated by herringbone structures of 4.62 – 4.64 nm of considerably lower density, and of a rope of 2.75 nm again. It can clearly been seen that two crystalline sheets of crystals are mixed and meet at angle of ~60° by forming an arrow, where each electron dense rope is separated by a less dense region of constant distance of 4.6 nm. This can best be described as disordered areas of molecular order but without long-range correlation. Similar patterns are observed by AMF in the presence of magnetite. Figure 12 depicts the fine structure of an unprocessed 30 nm x 30 nm image of a crystalline array of autovaccines (Ø = 4.0 x 10^{-4}, whereas Figure 13 shows one crystalline layer of autovaccines molecules where a molecular lattice (presumably cubic, could also be rectangular) is clearly visible. The inserts correspond to the electron diffraction pattern obtained from the same specimen. Figures 12 and 13 show almost absence of lattice defects and the presence of regular crystalline order. The sharp and symmetric reflections obtained by electron diffraction within this two dimensional array confirm that both the positional and orientational order are long-range. The 12 strongest reflections have been tentatively indexed on the basis of a body centred cubic lattice (bcc) with lattice repeats of a = 0.573 ± 0.042 nm, or on a distorted hexagonal pattern with two distinct lattice repeats of 0.543 ± 0.051 nm by 0.59 ± 0.05 nm with an angle of tilt of ~57° (Figure 14). For both structures the basic structural motif seems to be a dimer of the autovaccines. From the lattice repeats and the bilayer thickness measured from Figure 10 of 4.6 nm, we propose that the molecular

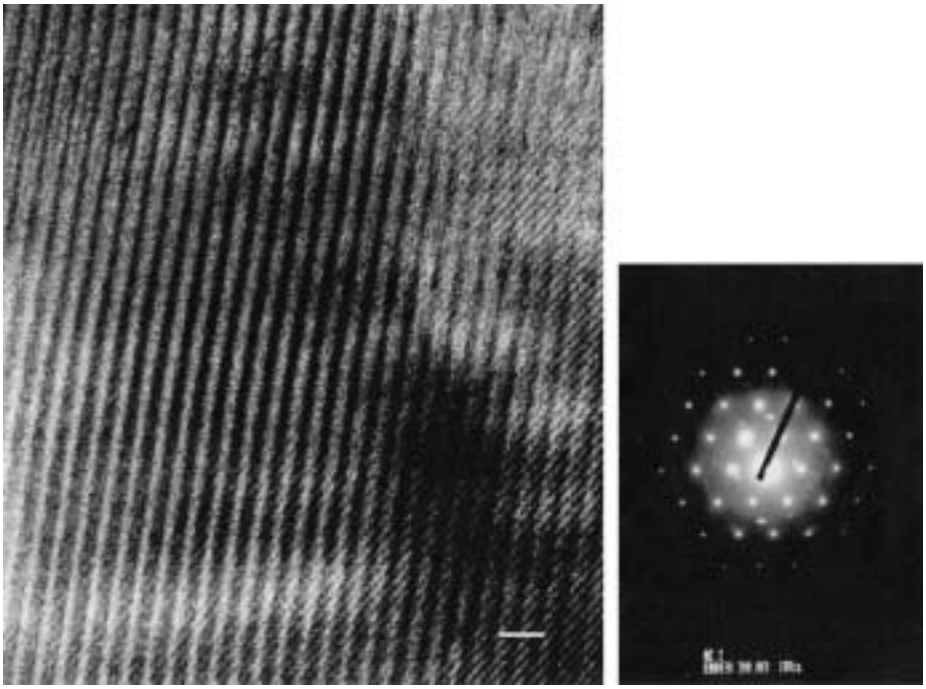

Figure 12: TEM image (left) and the corresponding electron diffraction pattern (right) of the image. Alternating rows of high and low zigzag molecules of autovaccines can be clearly seen. The bar size is 2.5 nm (*Faunce* and *Paradies*, unpublished results).

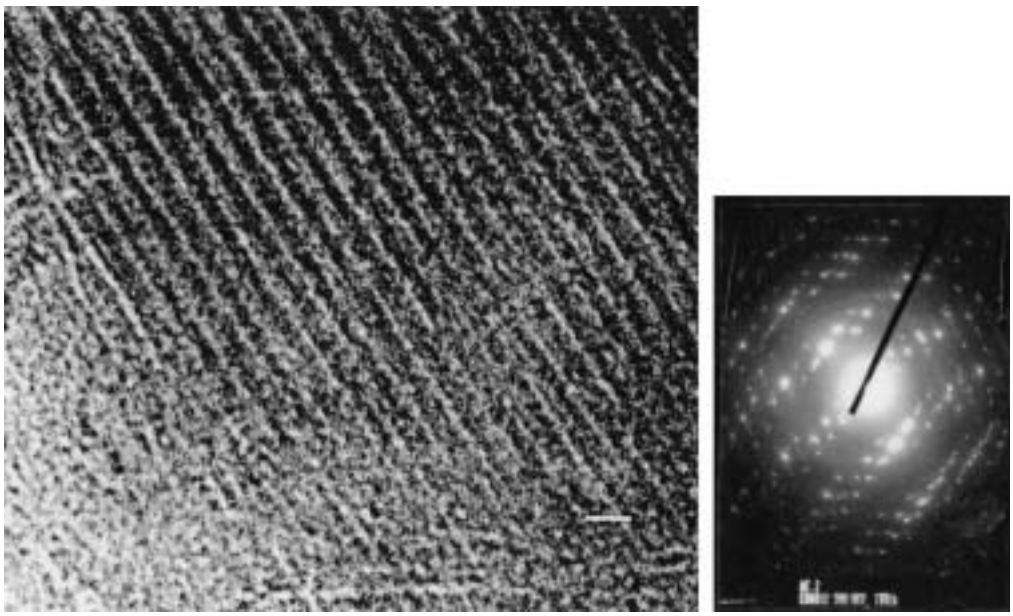

Figure 13: TEM image (left) and electron diffraction pattern (right) of superimposed crystalline lattices (unprocessed image of 33 nm x 33 nm. Three different lattices can be seen. The bar size is 2.5 nm (*Faunce* and *Paradies*, unpublished results).

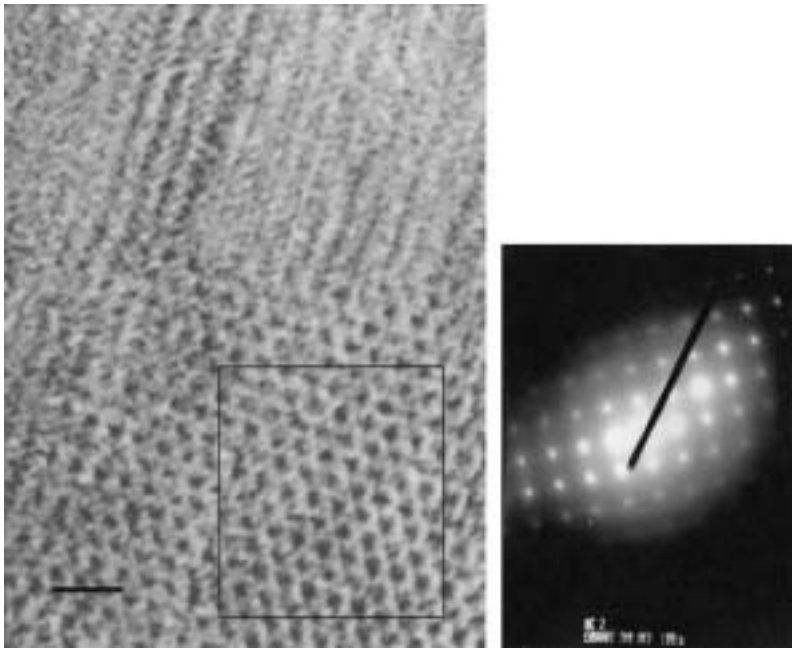

Figure 14: Highly ordered layer structure of autovaccines (left) in unprocessed molecular resolution and its electron diffraction pattern (right). A 30 nm x 30 nm image showing a defect molecular lattice (left). The sharp and symmetric reflections are indicative of long-range positional and orientational order (*Faunce* and *Paradies*, unpublished results)..

packing of the individual autovaccine molecule in the plane perpendicular to the long axis can be hexagonal (hcp), and that the autovaccine molecule are tilted toward nearest neighbours at angle of approximately 30°. From our data, it seems that the removal of the excess of counterions, e.g. NaCl, through tangential ultrafiltration (*Thies* et al., 2001; *Faunce* et al., 2001) plays a significant role in determining the multi-layered structure of the autovaccines and the formation of colloidal crystals. Particularly the influence of Ca^{2+}, Mg^{2+} and K^{+} ions play a dominant role in the formation and the substructure of the autovaccines as documented through the determination of the structure factors. In addition the particle number density determines whether a bcc or a fcc (hcp) lattice is formed as will be shown below. Apparently the acyl moiety of the autovaccines is, that determines the lattice parameters and symmetry that is compatible with close packing (*Kitaigorodskii*, 1961) gives the constraint imposed by specific counterions, and possibly the sugar backbone, too. Furthermore, the length of the fatty acid chains plays no severe role in the lattice parameters and symmetry, although it does have a limited effect on the details of the buckling superstructures for this class of autovaccines.

At high volume fraction ($4.15 \times 10^{-4} < Ø < 5.15 \times 10^{-4}$) and both ionic strengths (1.0 mM and 10.0 mM NaCl) and for $Ø = 4.75 \times 10^{-4}$ the x-ray spectra indicate the presence of long-range order (Figure 15). The assignment of the respective peaks to the crystal planes were made from comparison of the observed peak vectors according to

$$Q_{hkl} = \frac{2\pi}{\alpha}\left(h^2 + k^2 + l^2\right)^{1/2} \qquad (10)$$

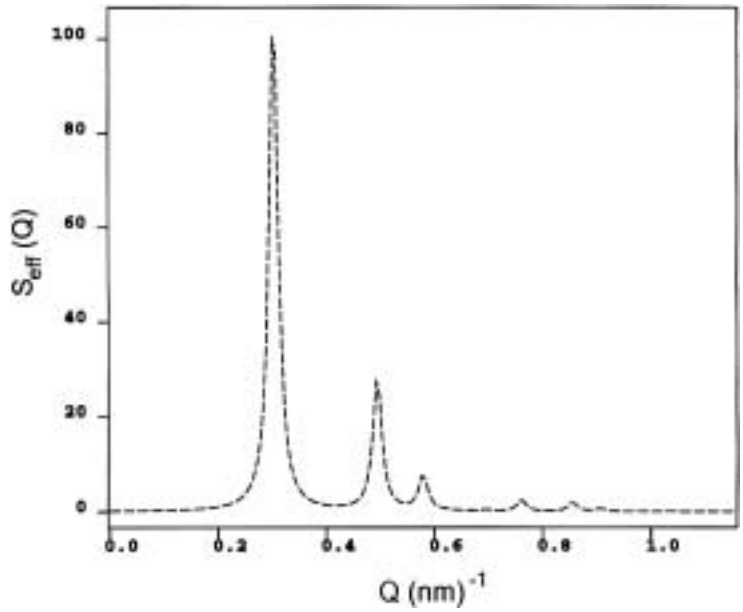

Figure 15: Small-angle-X-ray scattering, $S_{eff}(Q)$ vs. Q, obtained from autovaccines) dispersions at a volume fraction of $\varnothing = 4.75 \times 10^{-4}$ and 1.0 mM NaCl. The peak positions is assumed to be of a fcc type structure (*Faunce* et al., 2001).

where h, k and l are the Miller's indices and a is the unit cell size. The few peaks were assigned to be reflections originating from a face-centred cubic (fcc) lattice with a unit cell dimension of a = 57.25 ± 1.5 nm. The Bragg distances observed from the Q values using the Bragg equation $d = 2\pi/Q$ agreed with the corresponding values calculated from the sphere concentration. Due to the very few diffraction lines of the X-ray spectrum it is not possible to determine an appropriate space group unequivocally. Even with increasing volume fraction, no higher order peaks were found in the spectra and showed no definitive structure, e.g. at 1.0 mM NaCl and $4.15 \times 10^{-4} < Ø < 5.15 \times 10^{-4}$, strongly suggests that an ordered structure is present under this condition. However, no higher order peaks are found. The indication of long-range order behaviour of Lipid A (diphosphate) dispersions suggests that the degree of polydispersity associated with this charged system is tolerated. *Pusey* (1980) calculated the degree of polydispersity where colloidal crystals appear, and it did not exceed 0.07-0.11 (see above). Assuming that the time to form these structures of Lipid A (diphosphate) is related to the degree of polydispersity, it can be inferred that the increase in time of forming these colloidal crystals increases the degree of polydispersity.

The formation of colloidal crystals at volume fraction between $3.75 \times 10^{-4} < Ø < 4.15 \times 10^{-4}$ in the presence of 1.0 mM NaCl has also been observed and analysed by SAXS. Within this volume fraction regime the presence of long-range order can also be seen, but surprisingly the diffraction peaks are at different position (Figure 16). This X-ray spectrum was indexed on the basis of a bcc lattice with a = 36.14 ± 1.3 nm. From the X-ray spectra obtained at 1 mM NaCl and $Ø = 4.05 \times 10^{-4}$, it was assumed that the first peak corresponds

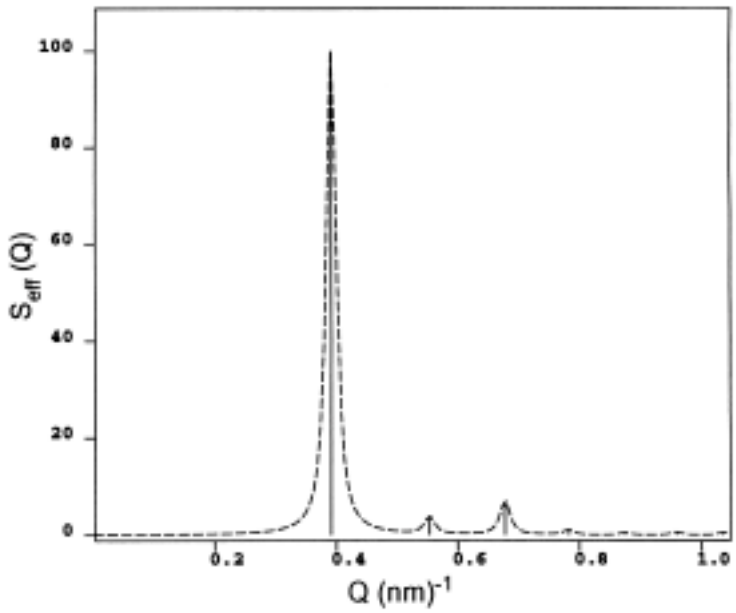

Figure 16: Small-angle X-ray scattering spectra, $S_{eff}(Q)$ vs. Q, obtained from autovaccines dispersions at a volume fraction of $\varnothing = 4.05 \times 10^{-4}$ and 1.0 mM NaCl. The peak positions is assumed to be of a bcc type structure (*Thies* et al., 2001, *Faunce* et al., 2001).

to that of the closest packed plane in the bcc structure, e.g. (110) having a spacing of 0.2458 nm^{-1}. Assuming that this first peak corresponds to the (110) planes, $d = d_{110}$, and for a bcc lattice, there should be two molecules per unit cell, and since the concentration is of Lipid A (diphosphate) is known, the molecular weight can be calculated according to

$$MW = (\sqrt{2} \cdot d_{110})^{1/3} \cdot c/2 \qquad (11)$$

From Equation (11) we calculated a molecular weight of 10.05×10^6 g/mol, which is consistent with the value found from light scattering and osmotic pressure experiments reported earlier. The molecular weight calculated from the fcc structure, which has four molecules in the unit cell, a value of 10.1×10^6 g/mol was found.

These two colloidal crystal forms apparently are in a sort of equilibrium when grown or appearing within a period of time of six to eight weeks. Increasing the subphase with Lipid A (diphosphate) at constant low ionic strength (1 mM or lower), we observe the formation of a fcc lattice in addition to the bcc lattice originally found. For both structures the diffraction lines are clearly distinguishable. Finally, after four weeks most of the colloidal crystals transformed to the fcc structure under this condition, if the concentration of the subphase of Lipid A (diphosphate) is kept constant ($\varnothing \cong 3.9 \times 10^{-4}$). Otherwise, a fraction of the fcc structure and the bcc structure will be present simultaneously.

It is noteworthy, that the quality of the diffraction data is strongly related to the sizes of the colloidal crystals of Lipid A (diphosphate) grown under deionised conditions. The relative intensity distribution (Figures 15 and 16) of the calculated and observed Bragg reflections, particularly those of the weak ones compared to the first order hkl

Bragg reflections, e.g. (110) or (111), are sensitive to variation in size of these colloidal crystals. The ultimate size and shape of the Lipid A (diphosphate) aggregate in form of a colloidal crystal, determines the geometrical arrangement, e.g. whether they have rounded, spherical or ellipsoidal or facetted shapes (hexagonal in shape), or as little cubic crystals, all observed in electron micrographs (TEM and SEM), and cannot not finely established presently but it is most likely.

Especially, for $0.1 \leq Q/Q_{110} \leq 0.75$ the Q dependence of the liquid phase and the crystalline bcc phase is very similar, and the peak in S(Q) for the liquid is close to $Q = Q_{110}$. This suggests a similarity in the structure of the liquid and the bcc crystal phase. But, taking the bcc structure, Q_{110}, to be at the first peak in S(Q), we would expect the second peak located at $Q = \sqrt{2} \times Q_{110}$, however, we notice a first minimum in S(Q) in the liquid state. Although we observe higher orders in the bcc structure, we only see a shallow peak in the liquid structure factor at $Q = 1.67 \times Q_{110}$, an indication that the wave vector dependence of the liquid dispersion of Lipid A (diphosphate) exhibits some common features with that for the longitudinal 110 lattice vibrations in the bcc crystal. It has been demonstrated by a number of authors (*Monovoukas* and *Gast*, 1989; *Okubo*, 1994; *Sirota* et al., 1982), that the bcc lattices are seen for systems which interact via long-ranged interactions, and this seems particularly true at low ionic strengths. A typically and sustained problem in colloidal systems is how to lower the ionic strengths. On the other hand, this system at 10 mM NaCl seems to be closer to the one for hard spheres than for one with the absence of ions, perhaps such a system is more sensitive towards the degree of polydispersity, and the observed degree of polydispersity can be one reason that the formation of long range order of a fcc lattice is inhibited, hence favours the formation of a bcc lattice (*Larsen* and *Grier*, 1997, *Cotter* and *Clark*, 1987). Furthermore, the very recent contribution by *van Roi* and *Hansen* (1997) offers an additional explanation, showing theoretically the coexistence of fluid-fcc and the fluid-bcc structures at very low ionic strength, is on energy terms very similar, since the free energy difference between fcc and bcc is much smaller than that between the fluid, and it is not possible to distinguish between fcc or bcc precisely. It is most likely, therefore, that the observations reported here are due to the existence of long-lived metastable colloidal crystallites at very low ionic strength.

ACKNOWLEDGEMENT

The long lasting patience of “feigenbaum” during the tangential ultrafiltration is greatly appreciated.

LITERATURE

Morbidity and Mortality Weekly Report. 46, 941-944. 1997.

Alexander, S., Chaikin, P.M., Grant, P., Morales, G.J., Pincus, P., and Hone, D.: Charge renormalization, osmotic pressure, and bulk modulus of colloid crystals. Theory. J. Chem. Phys. 80, 5776-5781 (1984).

Archibald, D.D. and Mann, S.: Template mineralization of self-assembled anisotropic lipid microstructures. Nature 364, 430 (1993).

Asher, S.A., Holtz, J., Weissmann, J., and Pan, G.: Mesoscopically periodic photonic-crystal materials for linear and nonlinear op-

tics and chemical sensing. MRS Bulletin 23, 44 (1998).

Belloni, L.: Electrostatic interactions in colloidal solutions:comparison between primitive and one-component models. J. Chem. Phys. 85, 519-526 (1986).

Belloni, L.: Inability of the hypernetted chain integral equation to exhibit a sigmoidal line. J. Chem. Phys. 98, 8080-8095 (1993).

Brandenburg, K., Mayer, H., Koch, M.H., Weckesser, J., Rietschel, E.T., and Seydel, U.: Influence of the supramolecular structure of free Lipid A on its biological activity. Eur. J. Biochem. 218, 555-563 (1993).

Clancy, S.F. and Paradies, H.H.: Double-chained cationic surfactants, transition states. Dependency on counterions and their physical implications. Recent Dev. Phys. Chem. 3, 607-731 (1998).

Clancy, S.F., Tanner, D.A., Steiger, P.H., Thies, M., and Paradies, H.H.: Micellar behavior of diastearyldimethylammonium hydroxide and chloride in aqueous solutions. J. Phys. Chem. 98, 11143-11156 (1994).

Cotter, L.K. and Clark, N.A.: Density fluctuation dynamics in a screened coulomb colloid: Comparison of the liquid and bcc crystal phases. J. Chem. Phys. 86, 6616-6621 (1987).

Din, Z.Z., Mukerjee, P., Kastowsky, M., and Takayama, K.: Effect of pH on solubility and ionic state of lipopolysaccharide obtained from the deep rough mutant of *Escherichia coli*. Biochemistry 32, 4579-4586 (1993).

Ernst, R.K., Yi, E.C., Guo, L., Lim, K.B., Burns, J.L., Hackett, M., and Miller, S.I: Specific lipopolysaccharide found in cystic fibrosis airway *Pseudomonas aeruginosa*. Science 286, 1561-1565 (1999).

Faunce, C.A. and Paradies, H.H.: Size separation of Lipid A diphosphate into colloidal crystals. Electron microscopy and stimulation. Physical Review Letters , in press (2002).

Faunce, C.A. and Paradies, H.H.: Solution and structural properties of colloidal Lipid A - diphosphate dispersions. J. Chem. Phys., in press (2002).

Glauser, M.P., Zanetti, G., Baumgartner, J.G., and Cohen, J.: Septic Shock: Pathogenesis. Lancet 338, 732-736 (1991).

Guinier, A. (Ed.).: Small-Angle Scattering of X-Rays (first edition). Wiley and Sons, New York (1955).

Hachisu, S., Kobayashi, Y., and Kose, A.: Phase separation in monodisperse lattices. J. Colloid Interface Sci. 42, 342-348 (1973).

Hansen, J.-P. and Hayter, J.B.: A rescaled MSA-structure factor for dilute charged colloidal dispersions. Mol. Phys. 46, 651-656 (1982).

Hansen, J.-P. and Mc Donald, I.R.: Theory of simple Liquids. Academic Press, New York (1976).

Hayter, J.B., Rivera, M., and McGroarty, E.J.: Neutron scattering analysis of bacterial lipopolysaccharide phase structure. Changes at high pH. J. Biol. Chem. 262, 5100-5105 (1987).

Hiltner, P.A. and Krieger, I.M.: Diffraction of light by ordered suspensions. J. Phys. Chem. 73, 2386-2389 (1969).

Hinze, U., Thies, M., and Paradies, H.H.: Template mineralization of ordered nanomaterials of copper and copper oxides in the presence of double-chained cationic Lipids (III). The Rigaku Journal 17, 9-19 (2000).

Kitaigorodskii, A. I.: Organic Chemical Crystallography. Consultans Bureau, New York (1961).

Klug, A., Franklin, R.E., and Humphreys-Owen, S.P.: The crystal structure of Tipula iridescent virus as determined by Bragg reflection of visible light. Biochem. Biophys. Acta 32, 203-219 (1959).

Kotra, L.P., Golemi, D., Amoro, N.A., Liu, G.-J., and Mobashery, S.: Dynamics of the lipopolysaccharide assembly on the surface of *Escherichia coli*. J. Am. Chem. Soc. 121, 8707-8711 (1999).

Larsen, A.E. and Grier, G.D.: Like-Charge Attractions in metastable colloid crystalloides. Nature 385, 230-233 (1997).

Luck, W., Klier, M., and Weslau, H.: Über Bragg-Reflexe mit sichtbarem Licht an monodispersen Kunststofflatices. Ber. Bunsenges Phys. Chem. 67, 75-85 (1963).

Luzzati, V., Vargas, R., Gulik, A., Mariani, P., Seddon, J.M., and Rivas, E.: Lipid polymorphism: A correction. The structure of the cubic phase of extinction symbol Fd- - consists of two types of disjointed reverse micelles embedded in a three-dimensional hydrocarbon matrix. Biochemistry 31, 279-285 (1992).

Mariani, P., Luzzati, V., and Delacroix, H.: Cubic phases of lipid-containing systems. Structure analysis and biological implications. J. Mol. Biol. 204, 165-189 (1988).

Medina-Noyola, M. and McQuarrie, D.A.: On the interaction of spherical double layers. J. Chem. Phys. 73, 6279-6283 (1980).

Monovoukas, Y. and Gast, A.P.: A study of colloidal crystal morphology and orientation via polarizing microscopy. Langmuir 7, 460-468 (1991).

Ochiai, T.: Salt-Sensitive growth of *Staphylococcus aureus*: Stimulation of salt-induced autolysis by multiple environmental factors. Microbiol. Immunol. 43, 705-709 (1999).

Ochiai, T.: *Staphylococcus aureus* produces autolysin-susceptible cell walls during growth in a high-NaCl and low-Ca2+ concentration medium. Microbiol. Immunol. 44, 97-104 (2000).

Okubo, T. and Kiriyama, K.: Static and dynamic light scattering of colloidal crystals of monodispersed Polystyrene particles. Ber. Bunsenges Phys. Chem. 100, 849-856 (1996).

Oosawa, P.: Biological Polyelectrolytes. Marcel Dekker, New York (1970).

Paradies, H.H., Faunce, C.A., Quitschau, P., and Zimmermann, K.: Liquid-like ordered colloidal suspensions of Lipid A diphosphate. The influence of Ca^{++}, Mg^{++} and K^{+} on the ordering of colloidal suspensions of Lipid A diphosphate in solution. J. Phys. Chem., in press (2002).

Paradies, H.H., Quitschau, P., Zimmermann, K., Thies, M., and Rusch, V.: Neutron scattering and modelling workshop: Neutron scattering of colloidal crystals of Lipid A and Lipid A derivatives. L6, 19.4-21.4. Conference Proceedings(2000).

Paradies, H.H., Quitschau, P., Zimmermann, K., Thies, M., and Rusch, V.: Self-assembly of Lipid A and analogues in solution to colloidal crystals. ACS National Meeting, Section Colloid and Surface Science: # 215. Conference Proceedings (2002).

Paradies, H.H., Rusch, V., and Zimmermann, K.: Kyberdrug as autovaccines with immune-regulating effects. US Patent Application No #11057(11057), pp. 1-60 (2000).

Pusey, P.N.: Liquids, freezing and glass transitions. North-Holland Publ., Amsterdam (1980).

Raetz, C.R.: Biochemistry of endotoxins. Annu. Rev. Biochem. 59, 129-170 (1990).

Raetz, C.R.: In: *Escherichia coli* and *Salmonella*: Cellular and molecular biology (Ed.: Neidhardt, F.C.). ASM Press, Washington D.C. (1996).

Seydel, U., Brandenburg, K., Koch, M.H., and Rietschel, E.T.: Supramolecular structure of lipopolysaccharide and free lipid A under physiological conditions as determined by synchrotron small-angle X-ray diffraction. Eur. J. Biochem. 186, 325-332 (1989).

Seydel, U., Labischinski, H., Kastowsky, M., and Brandenburg, K.: Phase behavior, supramolecular structure, and molecular conformation of lipopolysaccharide. Immunobiology 187, 191-211 (1993).

Sirota, E.B., Qu-Yang, D.H., Sinha, S.K., and Chaikin, P.M.: Complete phase diagram of a charged colloidal system: A synchrotron x-ray scattering study. Phys. Rev. Letters 62, 1524-1527 (1989).

Thies, M., Clancy, S.F., and Paradies, H.H.: Dynamic aspects of formation of synthetic membranes. Mat. Res. Soc. Symp. Proc. 463, 115-123 (1997).

Thies, M., Quitschau, P., Zimmermann, K., Rusch, V., Faunce, C.A., and Paradies, H.H.: Liquid-like ordered colloidal suspensions of Lipid A. The influence of Lipid A particle concentration. J. Chem. Phys. 116, 3471-3483 (2002).

van Roij, R.: Attraction or repulsion between charged colloids? A Connection with Debye-Hückel Theory. J. Phys. Condens. Matter 12, 263-267 (2000).

van Roij, R. and Dijkstra, M.: Phase Diagram of charged-stabilized colloidal suspensions: Van der Waals instability without attractive forces. Phys. Rev. 59, 2010-2025 (1999).

van Roij, R. and Hansen, J.-P.: Van der Waals-Like instability in suspensions of mutually repelling charged colloids. Phys. Rev. Letters 79, 3082-3085 (1997).

Verlet, L. and Hansen, J.-P.: Phase transitions of the Lennard-Jones System. Phys. Rev. 184, 151-161 (1969).

Verwey, E.J.W. and Overbeck, J.Th.G.: Theory of the stability of lyophobic colloids. Elsevier, Amsterdam (1948).

Wagner, N. J. and Klein, R.: Leading Contribution: the rheology and microstructure of charged colloidal suspensions. Colloid and Polymer Science 269, 295-319 (1991)